H. Yu, S. Chen, X. Yu, W. Zhang, C. Paravan, L.T. De Luca, R. Shen
Nickel Acetylacetonate as Decomposition Catalyst for HTPB-Based Fuels: Regression Rate Enhancement Effects
Fuel, Vol. 305, 2021, 121539 (10 pages)
doi:10.1016/j.fuel.2021.121539

Nickel acetylacetonate as decomposition catalyst for HTPB-based fuels: regression rate enhancement effects

Hongsheng Yu [a], Suhang Chen [a], Xiaodong Yu [a], Wei Zhang [a,*], Christian Paravan [b], Luigi T. DeLuca [b], Ruiqi Shen [a,*]

[a] School of Chemical Engineering, Nanjing University of Science and Technology, Nanjing 210094, China; Institute of Space Propulsion, Nanjing University of Science and Technology, Nanjing 210094, China

[b] Space Propulsion Laboratory (SPLab), Department of Aerospace Science and Technology, Politecnico di Milano, Milan, I-20156, Italy

[*] Corresponding author at: School of Chemical Engineering, Nanjing University of Science and Technology, No.200 Xiao Lingwei Street, Xuan Wu District, Nanjing, Jiang Su 210094, China.
E-mail: rqshen@njust.edu.cn (R. Shen), wzhang@njust.edu.cn (W. Zhang)

Abstract

This paper investigates the effects of nickel acetylacetonate, $Ni(acac)_2$, on the thermal stability and combustion of hydroxyl-terminated polybutadiene (HTPB)-based fuel formulations for hybrid rocket propulsion. The presented experimental results show that the addition of $Ni(acac)_2$ can intensely decrease the thermal stability of HTPB thus enhancing the solid fuel regression rate even at a small additive mass fraction: under an oxygen mass flux of 50 kg/m^{2}s, HTPB + 5 wt% $Ni(acac)_2$ shows a 25.5% increase over the non-loaded baseline. Kinetics analyses reveal that the catalytic effect is mainly induced by the Ni^{2+} in $Ni(acac)_2$ at the early stage of decomposition, and by the NiO produced from the oxidative decomposition of $Ni(acac)_2$ in the fuel final

degradation stage. On the other hand, the addition of $Ni(acac)_2$ decreases the combustion heat of HTPB-based fuels significantly and implies the accumulation of its decomposition products at the fuel regressing surface. Eventually, when the content of $Ni(acac)_2$ exceeds 5 wt%, the growth of regression rate slows down rapidly, and a performance detriment occurs at 40 wt%. This study verifies the catalytic effect of $Ni(acac)_2$ on polymer matrix for HTPB based fuels showing the attractive regression rate performance of this additive.

Keywords: HTPB, Catalytic pyrolysis, Nickel acetylacetonate, Regression rate, Hybrid rocket propulsion.

1. Introduction

The hybrid rocket is regarded as a promising candidate for several emerging applications (space tourism, suborbital flight, and small satellite orbital injection) thanks to its inherent safety, reliability, limited environmental impact, potential throttleability, and relatively low recurring costs [1, 2]. Thanks to its superior properties (such as excellent processability with high filling particle mass fractions, high elongation with good elastic recovery), hydroxyl-terminated polybutadiene (HTPB) has been the most commonly investigated polymeric solid fuel in the hybrid rocket field [1, 3-5]. However, the slow regression rate due to the difficult pyrolysis of this polyurethane has limited its practical application [2, 6]. For HTPB-based fuels, regression rate enhancement is typically pursued by loaded formulations including energetic fuels (micro-/nano-sized metals, mechanically activated powders, hydrides) [7-10] and oxidizers (as ammonium perchlorate) [6, 11, 12], and including high thermal

conductivity and high radiation absorption materials as carbon nanotubes and opacifiers [13, 14]. Of these strategies, the solid fuel loading with oxidants hinders the inherent safety of fuels, while the addition of metal powders can yield aggregation and agglomeration at the burning surface [10]. On the other hand, carbon-based additives feature a limited impact on the regression rate. Paraffin-based fuels offer faster regression rate than HTPB, but this is paid by lower mechanical properties: paraffin blending with reinforcing polymers is required to obtain suitable mechanical resistance, and this implies a ballistic response detriment [15]. HTPB-paraffin blends were proposed as a candidate solution to combine high mechanical properties with faster regression rates, yet the open-literature shows contrasting results when this solution is implemented [16-18].

In the propulsion field, transition metal elements (not including metal powders) have always been used as catalysts for oxidants like ammonium perchlorate [19-23]. On the other hand, the effect of these additives on the fuel matrix (i.e., HTPB) is rarely studied [24]. Numerous researchers have proved that some transition metal elements can promote the thermal decomposition of polymers. Moroi and Ciubanu found that Mn^{2+} can catalyze the overall pyrolysis process of polyurethanes, whereas Cu^{2+} reduces polymer initial thermal stability while catalyzing the final decomposition stage [25]. Transition metal chloride effects on the degradation temperature of polyurethane foam were discussed in Ref. 26.[6]The addition of ZnO nanoparticles dramatically reduces the thermal stabilities of polycarbonate-based polyurethane nanocomposites [27]. Laachachi et al. verified that the 15% and 20% TiO_2 can decrease the activation energy

of poly(methyl methacrylate) (PMMA) when the conversion degree exceeds 0.5 [28]. Thermal decomposition of HTPB is catalyzed by acetylacetonate complexes. Cardoso et al. demonstrated that Cu, Ni, Co, and Cr acetylacetonate complexes promote the pyrolysis of HTPB based fuels at high temperature [29]. However, this paper does not elucidate the catalytic process and combustion mechanism of fuels loaded with acetylacetonate complexes.

In the current work, nickel acetylacetonate ($Ni(C_5H_7O_2)_2$), $Ni(acac)_2$, is considered to enhance the regression rate of HTPB based fuels, by accelerating the pyrolysis of polymer matrix. The effects of $Ni(acac)_2$ on thermal stability, combustion heat, thermal conductivity, and regression rate of HTPB-based fuels were determined. Kinetic methods combined with analysis of the combustion products were used to clarify the catalytic process and combustion mechanism of fuel grains.

2. Experiment

2.1. Materials

The HTPB pre-polymer (average molecular weight of 2970 g/mol and -OH content of 0.787 mmol/g) was purchased from Liming Research & Design Institute of Chemical Industry Co., China. The dioctyl adipate (DOA, plasticizer), isophorone diisocyanate (IPDI, curing agent), and dibutyltin diacetate (TIN, curing catalyst) were obtained from Aladdin (Shanghai, China). The $Ni(acac)_2$ (purity 99%, density 1.455 g/cm^3, average number-based diameter of 46 μm), was supplied by Meryer Chemical Technology Co., Ltd (Shanghai, China). Scanning electron microscopy (SEM) images of the $Ni(acac)_2$ are reported in Fig. 1.

2.2. Sample preparation

Tested fuel formulations were manufactured at the Institute of Space Propulsion (ISP), Nanjing University of Science & Technology (NUST). A HTPB-based fuel with no additive served as the baseline for the study. $Ni(acac)_2$ loaded formulations featured 5, 10, 15, 20 and 40 wt% additive. The HTPB-based fuel consisted of 78.86 wt% HTPB pre-polymer, 13.04 wt% DOA, 7.67 wt% IPDI ([-NCO]/[-OH] = 1.08), and 0.43 wt% curing catalyst. Details on the formulations of HTPB + $Ni(acac)_2$ fuels are reported in Table 1. A schematic overview of the fabrication processes is shown in Fig. 1. The ZKJ-3 type vacuum mixer equipped with a 500 ml stirring cup was used to mix the reactants under vacuum (< 5 kPa) at 270 rpm. The HTPB pre-polymer, DOA, and TIN were mixed for 5 minutes. Following this step, $Ni(acac)_2$ was dispersed in HTPB, DOA, and TIN pre-mixture: mixing of the compound continued for 15 minutes. Finally, the IPDI was added to the mixture. The composition was then mixed under vacuum for 10 minutes. The stirred HTPB + $Ni(acac)_2$ slurry was cast into molds. The specimen for the ballistic analysis features a cylindrical shape with outer diameter (OD) of 19 mm, inner diameter (ID) of 16 mm, and length of 30 mm. Samples were cured for 24 hours at the temperature of 36°C. This step was then followed by a post-curing of 72 hours at 60 °C.

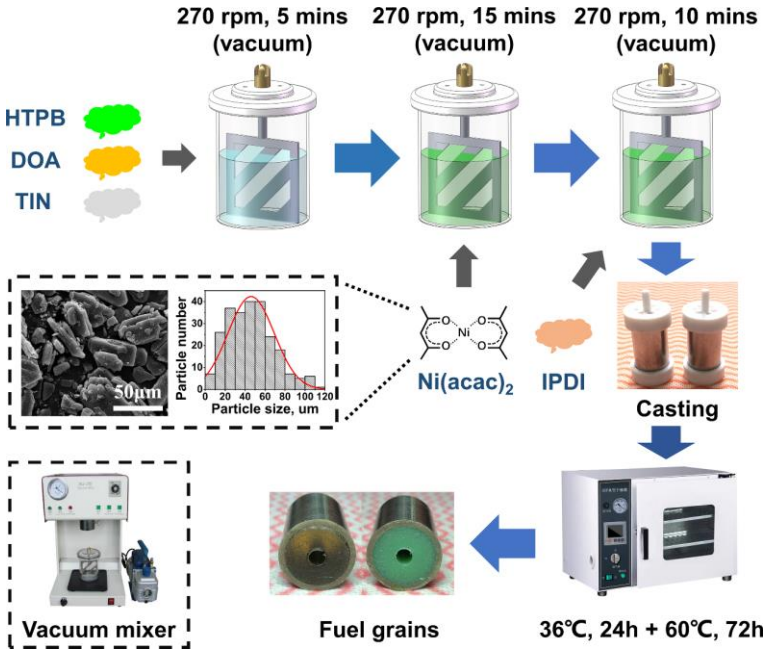

Fig. 1. Scheme of the phases in the preparation of HTPB + $Ni(acac)_2$ fuel grains.

Table 1. Composition of baseline and $Ni(acac)_2$ loaded formulations (ingredient contents are reported as mass fractions; HTPB-fuel ingredients normalized to 100%).

Formulation	HTPB	DOA	IPDI	TIN	$Ni(acac)_2$
Baseline	78.86	13.04	7.67	0.43	0
HTPB + 5 wt% $Ni(acac)_2$	74.92	12.39	7.29	0.41	5
HTPB + 10 wt% $Ni(acac)_2$	70.97	11.74	6.90	0.39	10
HTPB + 15 wt% $Ni(acac)_2$	67.03	11.08	6.52	0.37	15
HTPB + 20 wt% $Ni(acac)_2$	63.09	10.43	6.14	0.34	20
HTPB + 40 wt% $Ni(acac)_2$	47.32	7.82	4.60	0.26	40

2.3. Materials characterization methods

Field emission SEM (FESEM, Quanta 250FEG, USA) was operated at 10 kV coupled to an energy dispersive spectrometer (EDS), with a gold coating layer covering the specimens. FESEM + EDS enabled to evaluate the morphological structure of $Ni(acac)_2$, and the additive dispersion in HTPB + $Ni(acac)_2$. FTIR spectrometer

(Thermo Scientific Nicolet iS10, USA) and microcomputer automatic calorimeter (IKA C2000, Germany) were used to determine the molecular structure and combustion heat of pristine $Ni(acac)_2$, baseline, and loaded formulations. Differential scanning calorimetry (DSC)/thermogravimetry (TG) (Netzsch STA449C, Germany) was performed in air (50 mL/min), with a heating rate of 10° C/min to characterize the thermal behavior of all the fuels. DSC/TG scans with a heating rate of 5, 10, 15, and 20° C/min were performed on the baseline and HTPB + 15% $Ni(acac)_2$ in the temperature range 35° C to 700° C. Two fuel disks (50 mm OD, 13 mm height) were tested in a hot disk thermal analyzer (Hot Disk TPS2500, Sweden), equipped with a 6.40 mm radius Kapton sensor at 298 K. X-ray diffraction (XRD, Bruker D8, Germany) with Cu-K α radiation was employed to analyze the combustion products of pristine $Ni(acac)_2$, and HTPB + 15/40% $Ni(acac)_2$ composites.

2.4. Hybrid propulsion combustion system

As shown in Fig. 2 (schematic), a 2D-radial hybrid burner, based on the original design by the Space Propulsion Laboratory (SPLab) of Politecnico di Milano, was used to perform combustion tests on prepared fuels [10]. Further views of the facility are reported in Fig. S1, details on the facility are reported elsewhere [10,15] . Gaseous oxygen was used as oxidizer. A mass flow rate of 3 g/s was axially injected into the grain port. The oxidizer injector is designed to grant optical access to the tested specimen head-end, thus providing the possibility to track the central port diameter during the combustion. An automatic system combined with solenoid valves and pressure transducer-controlled chamber pressure granting a quasi-steady value of 1.0

MPa. A B/KNO_3 (40/60 wt%) primer charge was ignited by laser, providing a non-intrusive system for specimen ignition. The burning process of the cross-section was recorded by a high-speed camera operating at 500 fps. A scheme of the injector implementation and optical path for the visualization of the burning strand head-end is reported in Fig. 2. Gaseous nitrogen was used to interrupt the combustion before complete consumption of the fuel. A time-resolved technique was used for the regression rate (r_f) determination. This data reduction procedure enables the identification of relevant ballistic parameters (including the oxidizer mass flux, G_{ox}). Full details on the method are reported elsewhere [9, 13]. The non-loaded HTPB is taken as baseline for the relative grading of the tested formulations. Five combustion tests were performed for each formulation. Single test data were collapsed in an ensemble average curve enabling the definition of error bars based on standard deviation.

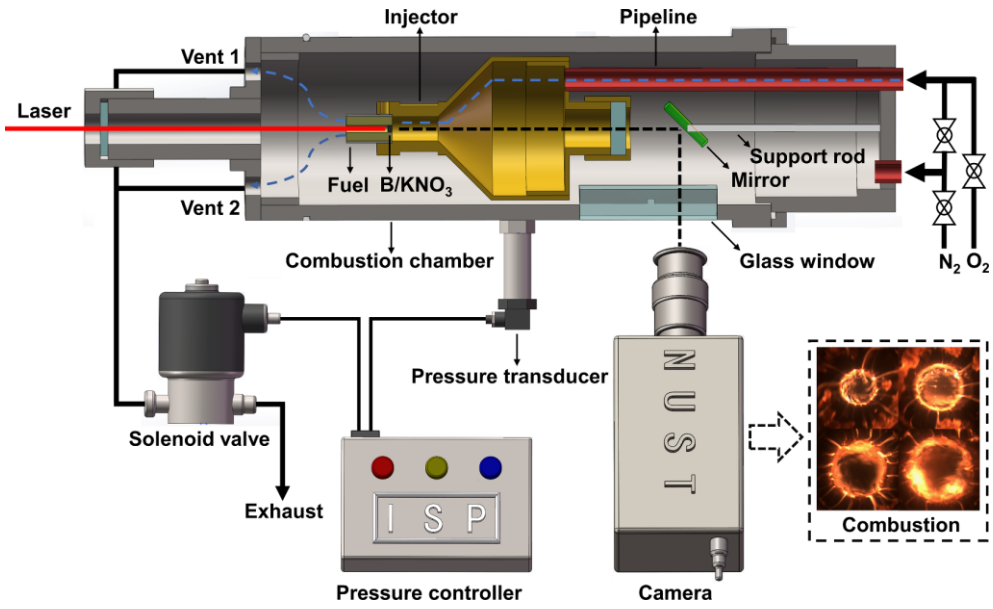

Fig. 2. Schematic of the 2D-radial hybrid burner.

2.5. Kinetic methods

Kinetic analyses were performed by DSC/TG scans at different heating rates. Two model-free non-isothermal methods were used for the data reduction, the distributed activation energy model (DEAM) and the Kissinger method were adopted to evaluate the activation energy (E) and frequency factor (A). The DAEM assumes that many irreversible first-order parallel reactions with different rate parameters occur simultaneously in determining the activation energy [30, 31]. The initial form of DAEM can be written as:

$$1-\alpha=\int_0^{\infty} exp\left(-A\int_0^t exp\left(-\frac{E}{RT}\right)dt\right)f(E)dE \tag{1}$$

$$\alpha=\frac{\int_0^t H\,dt}{\int_0^{t_f} H\,dt} \tag{2}$$

$$\int_0^{\infty} f(E)\,dE=1 \tag{3}$$

In the Eqs. 1-3, α is the conversion degree, R represents the ideal gas constant, T is the absolute temperature, $f(E)$ is the activation energy distribution curve, and H is the heat flow measured by DSC. Miura and Maki [32] simplified the original DAEM and expressed it as:

$$ln\left(\frac{\beta}{T^2}\right)=ln\left(\frac{AR}{E}\right)+0.6075-\frac{E}{RT} \tag{4}$$

with β indicating the heating rate. The basic equation of the Kissinger method [33] can be presented as:

$$ln\left(\frac{\beta}{T_m^2}\right) = ln\left(\frac{AR}{E}\right) - \frac{E}{RT_m} \quad (5)$$

where T_m represents the temperature peak of the DTG curve. In the proposed models, E can be obtained from the slope of the regression lines of $\ln(\beta/T^2)$ vs. $1/T$ for DAEM, and from $\ln(\beta/(d\alpha/dT))$ vs. $1/T_m$ for the Kissinger method. In the analyses, the value of A is determined by the intercept of regression lines.

3. Results and discussion

In this Section experimental results will be discussed for both the pre- and the burning phases. Composite characterization is introduced first, then combustion performances are discussed.

3.1. Composite characterization

3.1.1 FTIR spectrum analysis

Results from the FTIR analyses are shown in Fig. 3. The presented data include the characteristic peaks of the pristine $Ni(acac)_2$, together with the evidence from the HTPB + $Ni(acac)_2$ composites. Bands in the range 700-580 cm^{-1} show sensitivity to the nature of the metal. A peak at 669 cm^{-1} is assigned to the Ni-O stretching, while the one observed at 652 cm^{-1} is probably due to ring deformation of the organic moiety [34]. In the spectrum, the peak at 1660 cm^{-1} belongs to the keto-enol tautomerism of acetylacetonate, while what is seen at 3349 cm^{-1} corresponds to the presence of crystalline water introduced during the preparation of the pristine material [35, 36]. Focusing on the non-loaded HTPB, C=C stretching is noted at 1640 cm^{-1}, while the characteristic C=O band of the plasticizer is responsible for the peak at 1730 cm^{-1}. With

the addition of $Ni(acac)_2$, the intensity of characteristic peaks belonging to plain HTPB reduces significantly.

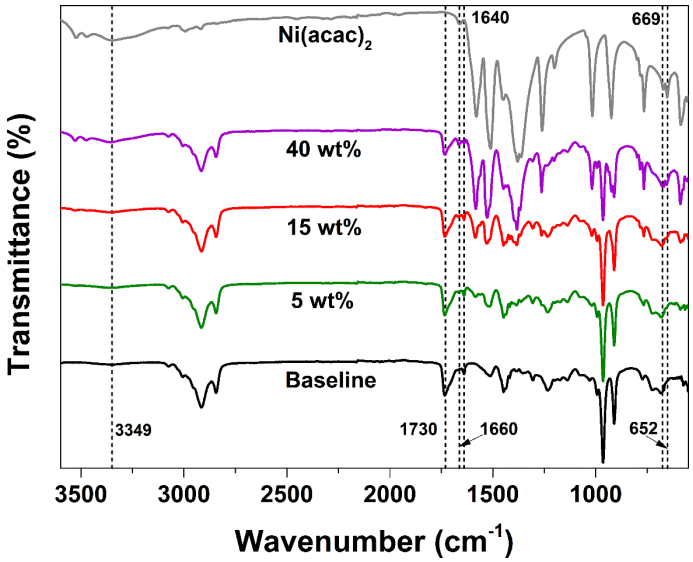

Fig. 3. FTIR spectra of the pristine $Ni(acac)_2$ and non-loaded/loaded HTPB-based formulations.

3.1.2 Thermal analysis

Thermal behavior characterization of the pristine $Ni(acac)_2$ and HTPB-based composites is shown in the Fig. 4. The weight loss of $Ni(acac)_2$ below 120°C is assigned to the departure of crystallization water, which corresponds to an endothermic peak at 111°C [35, 37, 38]. This is consistent with the spectral analysis results in Fig. 3. The large mass loss of the additive in the temperature range 120-395 °C is related to the multi-step decomposition of the acetylacetonate species, the main exothermic peak of this stage is at 375°C and ultimately leads to the formation of a residual product (22.4%) consisting of metallic Ni and NiO [35, 37]. For this reason, TG traces for loaded HTPB-based fuels show a residual mass for temperatures > 600°C (see Fig 5a).

The baseline fuel exhibits two mass loss stages corresponding to the exothermic

reactions whose peak temperature is at 205°C and 456°C. The first weight loss can be attributed to the oxidative decomposition of the plasticizer, while the second one is due to the depolymerization and decomposition of the remaining polybutadiene [16]. With the increase of $Ni(acac)_2$ mass fraction, the main exothermic peak (T_p) of the HTPB-based fuels is shifted from 456°C to 438°C, and the end temperature (T_f) of the decomposition reaction is significantly reduced (from 631°C to 580°C). Fig 5b depicts the differences between corresponding pairs of T_p and T_f values for pure HTPB fuel and HTPB + $Ni(acac)_2$ composites. Achieved data testify that $Ni(acac)_2$ catalyzes the pyrolysis of the cured HTPB matrix. Under the investigated conditions and catalyst contents, this catalytic effect increases for increasing $Ni(acac)_2$ mass fraction. Nevertheless, the main exothermic peak of the $Ni(acac)_2$ is observed to shift from 375°C to 367°C at low content (5 wt%), while it is hidden by the main exothermic peak of the HTPB matrix for larger mass fractions. In particular, for the 40 wt% load, the exothermic peak is eventually increased to 487°C. These results indicate that the decomposition by $Ni(acac)_2$ is catalyzed at low content (5 wt%), but the opposite effect is achieved at relatively high content ($\geqslant$ 20 wt%). ~~Overall,~~ The above results show that the presence of $Ni(acac)_2$ can greatly lower the decomposition temperature of HTPB-based fuels.

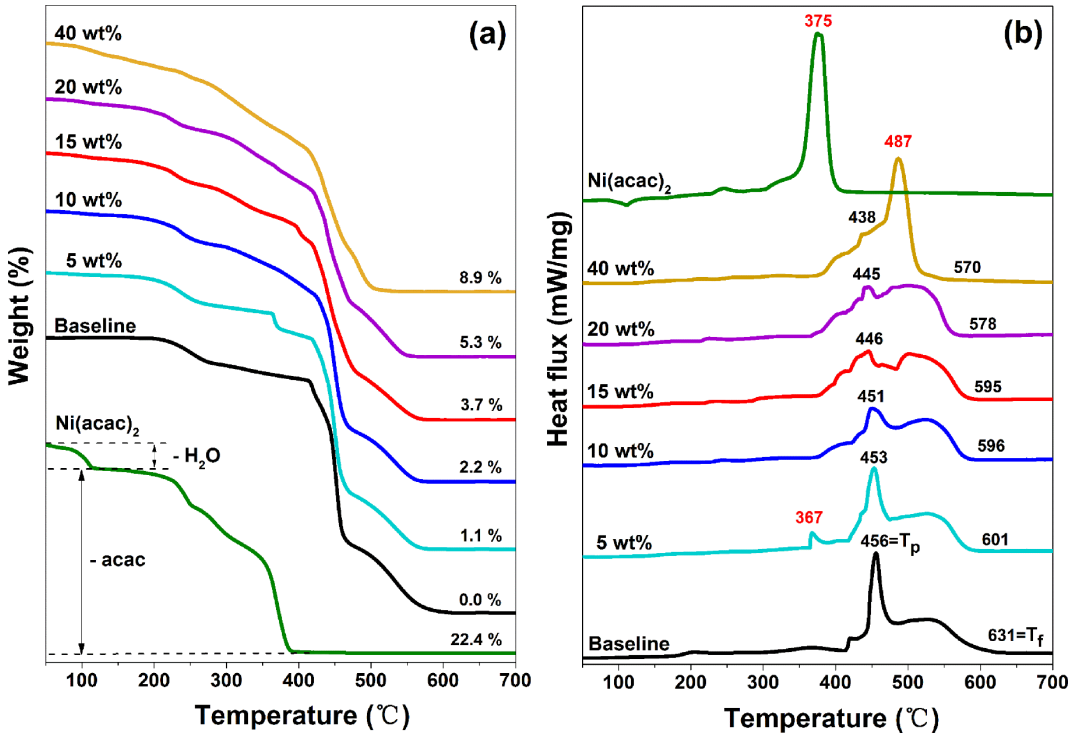

Fig. 4. Thermal analysis of pristine $Ni(acac)_2$ and non-loaded/loaded HTPB-based fuels: (a) TG, (b) DSC.

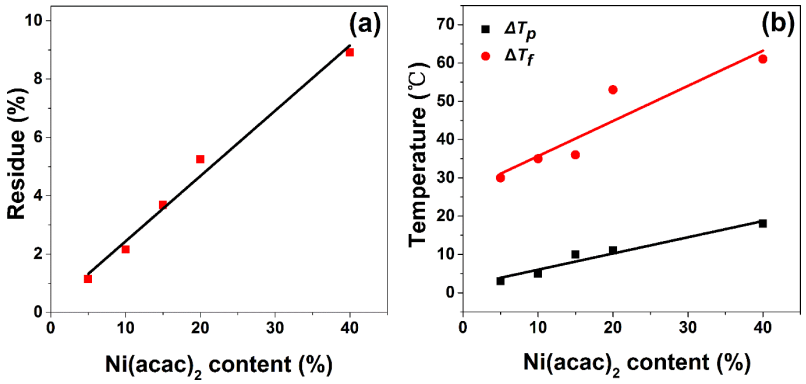

Fig. 5. Thermal analysis of pristine $Ni(acac)_2$ and non-loaded/loaded HTPB-based fuels: (a) residual mass after complete fuel decomposition, (b) difference between peak temperature (ΔT_p) and end temperature (ΔT_f) for pure HTPB and HTPB + $Ni(acac)_2$.

3.1.3 Combustion heat and thermal conductivity characterization

The combustion heat and thermal conductivity of the investigated fuels were determined to provide a deeper insight into their burning performance (Fig. 6a). The

use of $Ni(acac)_2$ yields an increase in the thermal conductivity of the HTPB-based composites (Fig. 6a). The baseline formulation provides a conductivity of 0.1992 W/mK, which is consistent with the open literature data [13, 39]. Nevertheless, because the combustion heat of $Ni(acac)_2$ is less than half of the corresponding value for non-loaded HTPB (18005 J/g vs. 42466 J/g), the addition of $Ni(acac)_2$ yields a decrease in the combustion heat for HTPB + $Ni(acac)_2$ composites. An XRD pattern of the residuals for $Ni(acac)_2$ in the combustion process is reported in Fig. 6b. The XRD pattern reveals that the metal in $Ni(acac)_2$ is not completely oxidized in the combustion heat test. Considering the characteristics of the XRD analysis, the actual content of Ni in the combustion products may be much higher than the 45.9% identified by the pattern of Fig 6b. This result partially explains the decrease of combustion heat in loaded formulations. Overall, the addition of $Ni(acac)_2$ for regression rate enhancement requires a proper trade-off for the identification of a suitable mass fraction of the additive.

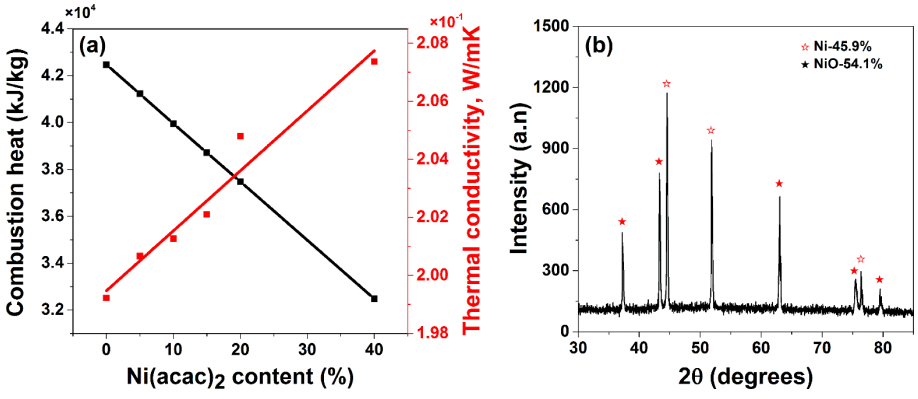

Fig. 6. Non-loaded HTPB and HTPB + $Ni(acac)_2$: (a) Combustion heat and thermal conductivity of prepared fuels; (b) XRD analysis of $Ni(acac)_2$ powder after combustion heat testing.

3.1.4 Combustion performance

An overview of the combustion process for selected fuel formulations is reported in Fig. 7, where t_i indicates the ignition time. A more detailed comparison, including the combustion process images of all composites is shown in Fig. S2. In Fig. 7 (and in Fig. S2), all the combustion images are captured enforcing the same operating parameters. The relative ballistic grading of the tested formulations is reported in Fig. 8 (r_f (G_{ox}) and percent r_f differences between the baseline and the $Ni(acac)_2$-loaded fuels). A qualitative analysis of the burning process (Fig. 7) shows that the addition of $Ni(acac)_2$ leads to a brighter image than that observed pure HTPB. Since the presence of $Ni(acac)_2$ can greatly promote the decomposition of fuel grains, it may be due to the accelerated pyrolysis of fuels during the burning process, resulting in more intense combustion. In addition to this, the presence of Ni provides radiating particles augmenting the image brightness. Diameter growth in time suggests a faster regression rate (i.e., larger diameter for the same time elapsed from t_i) for the $Ni(acac)_2$-loaded formulations featuring additive loading lower than 40 wt%. According to the images reported in Fig. 7 and Fig. S2, the fastest regression rate is achieved by HTPB + 15 wt% $Ni(acac)_2$, though with faint (if any) increase with respect to HTPB + 5 wt% $Ni(acac)_2$ (see the partially overlapped error bars). On the other hand, when the content of additive rises above 20% , the combustion process starts appearing slower, with a generally poorer quality (as observed by recorded images). Large fuel slivers ~~fragments~~ appeared during the combustion process in HTPB + 40 wt% $Ni(acac)_2$， indicating the fragmentation in the combustion of the fuel grain.

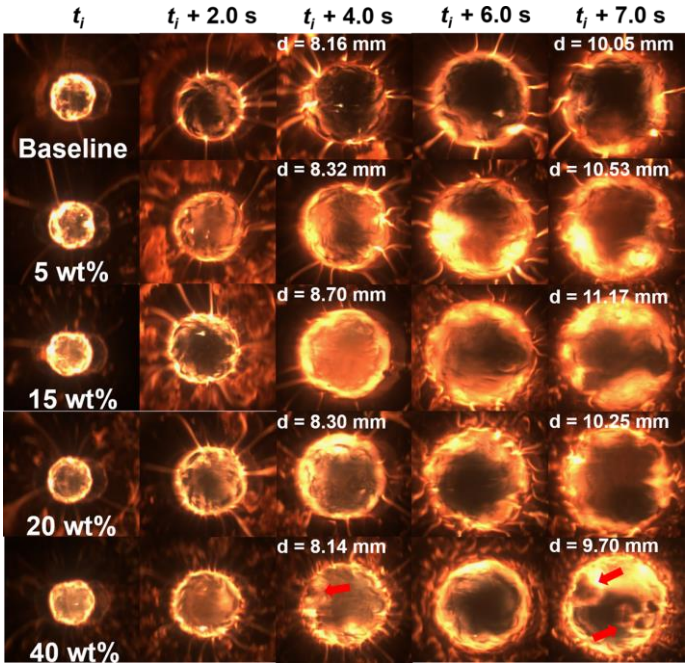

Fig. 7. Regression process of the non-loaded and loaded HTPB-based formulations (gaseous oxygen, 3 g/s, 1.0 MPa).

Fig. 8a describes the instantaneous $r_f(G_{ox})$ of pure HTPB and HTPB + $Ni(acac)_2$. The regression rate has been calculated based on the analysis of the sequence of combustion images and their corresponding burning surface recognition results (as shown in Fig. 7 and Fig. S2). Each curve is the average of 5 runs measured under the same conditions, and the error bar represents the standard deviation of measurements. Fig. 8b shows the regression rate increase of HTPB + $Ni(acac)_2$ composites relative to the baseline. The achieved ballistics responses can be compared with the performance of paraffin-based fuels burning under similar operating conditions by the data reported in Table 2 Fig. S3 ~~To further compare the regression rate increase of $Ni(acac)_2$ loaded formulations, paraffin, one of the most commonly used fuel matrix in the hybrid propulsion field, was tested under the same conditions and compared with the pure HTPB fuel. Its regression rate curve is presented in Fig. S3~~. The reported paraffin data

consider a macro-crystalline wax with melting point of 58.3°C (Sinopec). The full regression rate details and power law approximation of r_f vs. G_{ox} ($r_f = a_r . G_{ox}^{n_r}$) are shown in Table S1. All the tested fuel formulations show a n_r in the range 0.5 to 0.7 testifying a convective heat transfer mechanism with contributions from the radiation heat transfer.

Compared to the high oxidizer mass flux region, HTPB + $Ni(acac)_2$ composites exhibit more significant regression rate increases for relatively low oxidizer mass flux values: percent increases of 25.5%, 26.7%, 28.2%, 16.2% and -5.9% are achieved at G_{ox} = 50 kg/m^{2}s for 5%, 10%, 15%, 20%, and 40% $Ni(acac)_2$ respectively. Regression rate enhancement shows a faint dependence from the additive mass fraction in the fuel for $Ni(acac)_2$ loads < 20 wt%, and reaches its peak at 15 wt%. Starting from 20 wt% of $Ni(acac)_2$, the combustion performance of the fuel is lowered, even showing a regression rate decrease over the baseline at HTPB + 40 wt% $Ni(acac)_2$ composite. With respect to ~~Relative to~~ pure HTPB and $Ni(acac)_2$ loaded fuels, paraffin shows faster regression rates. However, this performance is obtained with extremely poor mechanical properties, making this fast-regressing fuel unsuitable in practical applications [40-42]. $Ni(acac)_2$ can act as an additive in the HTPB-based fuels also in the case of HTPB + paraffin blends or other multi-additive compositions. For example, in a fuel system composed of 40 wt% paraffin particles and 60 wt% HTPB, adding 7.6 wt% copper acetylacetonate to HTPB can increase the regression rate of the entire fuel by 82% at G_{ox} = 5 kg/m^{2}s [29].

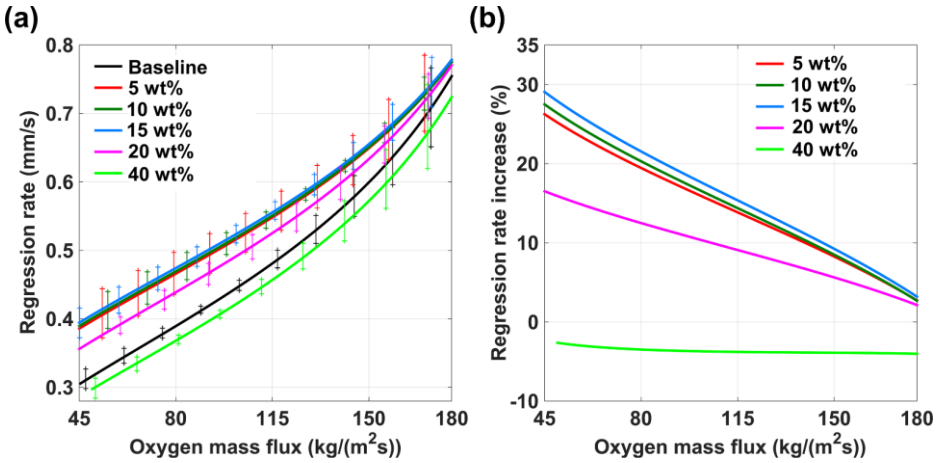

Fig. 8. HTPB-based fuels burning in gaseous oxygen: (a) regression rate, and (b) percent regression rate increase vs. oxygen mass flux.

Table 2. Details of the regression rate of the tested formulations: percent increases are evaluated with respect to the baseline.

	Regression rate (mm/s)		Regression rate increase (%)	
G_{OX} (kg/m^{2}s)	50	150	50	150
Baseline	0.317	0.599	-	-
5% wt%	0.398	0.649	25.5	8.3
10% wt%	0.402	0.651	26.7	8.6
15% wt%	0.406	0.655	28.2	9.3
20% wt%	0.368	0.633	16.2	5.7
40% wt%	0.298	0.572	-5.9	-4.5
58# paraffin	0.985	2.462	211	311

*G_{OX} - oxygen mass flux.

3.2. Thermal decomposition kinetics and combustion mechanisms

3.2.1 Kinetics for baseline and HTPB + 15% Ni(acac)$_2$

To further confirm the catalytic effect of Ni(acac)$_2$ on HTPB based fuels, the pure HTPB and HTPB + 15% Ni(acac)$_2$, which exhibits the fastest regression rate under the

investigated conditions, are compared by their activation energy. The DEAM method is employed based on DSC data (see Fig. S4) to calculate the kinetic parameters at different conversion degrees, and their variation trend and corresponding values are shown in Fig. 9 and Table S2. Kinetic parameters are evaluated for $0.25 \leqslant \alpha \leqslant 0.95$. In Fig. 9, the E of HTPB + 15% $Ni(acac)_2$ composite slightly decreases for $0.5 \leqslant \alpha \leqslant 0.7$, while it is drastically reduced for other conversion degrees. It can be inferred that the $Ni(acac)_2$ has a catalytic effect on the early and final stage of decomposition of HTPB based fuels. Schubert et al. report that the metal in $Ni(acac)_2$ exists as Ni^{2+} in the early stages of the heating process, and is then turned into Ni and NiO before getting fully converted into NiO at a high temperature [35]. Therefore, during the pyrolysis of HTPB + $Ni(acac)_2$ composites, Ni element exists as Ni^{2+} and NiO in the early and final stages. And there is a transformation from Ni^{2+} to NiO in the middle stage, showing the existence of relevant Ni. So, it can be concluded that the Ni^{2+} and NiO can catalyze the fuel grains drastically, while Ni has a weak (if any) catalytic effect.

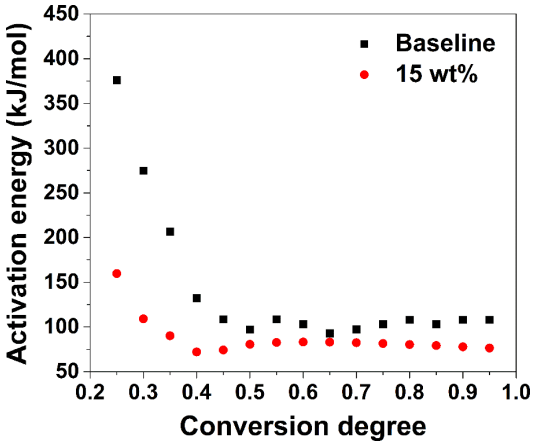

Fig. 9. Activation energy vs. conversion degree as evaluated by DEAM method for baseline and HTPB + 15% $Ni(acac)_2$.

3.2.2 Kinetics for polybutadiene component in baseline and HTPB + 15% Ni(acac)$_2$

Results from Sec. 3.1.2 suggest that polybutadiene is the fuel component ruling the decomposition process of the HTPB-based fuels. Because of the low pyrolysis temperature of Ni(acac)$_2$, the decomposition process (10° C/min) of HTPB + 15% Ni(acac)$_2$ above 450 °C is attributed to the degradation of polybutadiene component. Peak temperatures of the DTG curves (see Fig. S5) are used in the Kissinger method as input data (Eq. 5) to calculate E and A. As shown in Fig. 10, the HTPB + 15% Ni(acac)$_2$ composite with a heating rate of 10° C/min is used as an example to describe the peak locations. The kinetic parameters for polybutadiene in the baseline fuel and HTPB + 15% Ni(acac)$_2$ are listed in Table 3. From the calculated values of E, it can be observed that the average activation energy of polybutadiene component in HTPB + 15% Ni(acac)$_2$ has been lowered by 54% with respect to the baseline. This gap in the activation energy values suggests that Ni(acac)$_2$ can reduce the thermal stability of polybutadiene thus playing a catalytic role in the decomposition process. Such an outcome is consistent with the results presented in Sec. 3.1.2 and Sec. 3.2.1.

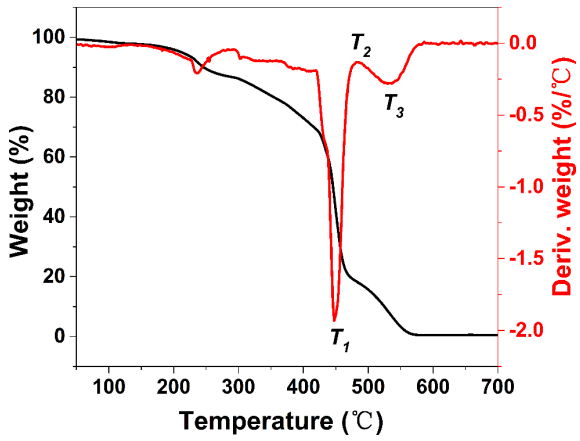

Fig. 10. TG and DTG curves of HTPB + 15% Ni(acac)$_2$, β = 10° C/min.

Table 3. Kinetic parameters obtained by the Kissinger method for polybutadiene component in baseline and HTPB + 15% $Ni(acac)_2$.

Samples		E (kJ.mol^{-1})	ln A (S^{-1})	R^2
Baseline	T_1	204.4	32.7	0.9995
	T_2	377.0	59.4	0.9999
	T_3	119.9	15.0	0.9501
	Average	233.8	35.7	
15 wt%	T_1	90.2	13.4	0.9985
	T_2	150.9	22.7	0.9896
	T_3	83.2	10.2	0.9994
	Average	108.1	15.4	

3.2.3 Combustion mechanisms

HTPB + 15% $Ni(acac)_2$ is used to testify the homogeneity of the prepared fuel grains, as shown in c0 of Fig. 11. The pre-burning morphology of all HTPB -based composites is shown in Fig. S6: $Ni(acac)_2$ is evenly distributed in HTPB matrix. The surface morphology of quenched fuel grains in selected formulations is shown in Fig. 11a-d, which reveal the state of the burning surface. The burning surface morphology of all composites is shown in Fig. S7. Compared to the plain HTPB, the loaded formulations feature accumulation of additive decomposition products at the regressing surface. This effect is more and more marked as the $Ni(acac)_2$ content is increased. The EDS mapping (c1 in Fig. 11) show that the blanket is composed of abundant C, widely distributed Ni, and little O.

The XRD spectrum is used to characterize the composition of melting layer near the burning surface, especially, the 15% and 40% $Ni(acac)_2$ composites are chosen as the specimen. Fig. 11-e1 exhibits the spectrum of pristine $Ni(acac)_2$, which is compared

with Fig. 11e for confirming the existence of $Ni(acac)_2$ in the surface layers. Fig. 11e reveals that the burning surface and adjacent melting layer contains much metal Ni, moderate elemental C, a little $Ni(acac)_2$, and less NiO. The XRD spectra indicate that the combustion surface is mainly covered by elemental C and metal Ni, instead of NiO. This is because the presence of carbonaceous species in metal-organic salt precursors can induce strong Ni^{2+} reduction to purely metallic species, and the blockage effect caused by fuel evaporation reduces the possible reaction of Ni with oxygen [2, 35]. Further, according to the analysis of Fig. 6b, $Ni(acac)_2$ is also difficult to be burned completely, ultimately leading to more metal Ni instead of NiO at the burning surface. The mixture of Ni and NiO covers the burning surface, inhibiting the pyrolysis and gasification of fuels, eventually causing part of the fuel to be carbonized and forming element C. The low content of $Ni(acac)_2$ is due to the undecomposed raw material that close to the melting layer near the burning surface. The above results are consistent with the analysis of Fig. 11-c1. Since the content of NiO is less than that of Ni on the burning surface, the content and distribution range of element O are also less than element Ni. The C element in Fig. 11-c1 comes from the C element in the pristine and partially pyrolized fuel. Too little N element in the fuel grains is hard to be detected.

According to the above analysis, Fig. 11f summarizes the combustion process of HTPB + $Ni(acac)_2$ composite. During the burning process, the $Ni(acac)_2$ in the melting layer decomposes into the metal Ni and (small amounts of) NiO. Compared with the gasified fuel, it is difficult for Ni and NiO to get entrained in the flow, thus these products of $Ni(acac)_2$ reaction are eventually accumulated at the burning surface.

Owing to the blockage effect of evaporated fuel on gaseous oxygen, the oxidation of Ni is slowed down, and Ni remains on the burning surface. The deposited Ni and NiO will inhibit the pyrolysis and gasification of the fuel, causing part of the fuel to be carbonized and forming element C. Ultimately, the element C, metal Ni, and NiO cover the burning surface, as shown in Fig. 11b-d and Fig. S7.

Originated from the catalysis by $Ni(acac)_2$ on HTPB-based fuels, only 5 wt% $Ni(acac)_2$ already enhances the regression rate by 25.5% at G_{OX} = 50 kg/m^{2}s. However, with the introduction of relatively high $Ni(acac)_2$ mass fractions, a reduction of combustion heat together with the insurgence of surface phenomena exhibit an increased inhibitory effect on combustion. Hence, regression rate enhancement shows a faint dependence from the additive mass fraction in the fuel for $Ni(acac)_2$ loads < 20 wt%, and reaches its peak at 15 wt%. Starting from 20 wt% of $Ni(acac)_2$, the combustion performance of the fuel is lowered, and a regression rate detriment with respect to the baseline is achieved for HTPB + 40 wt% $Ni(acac)_2$. Combining the characterization results of Fig. 11 with Fig. 7, we can conclude that the incomplete combustion in 40% loaded formulation originated from the severe coverage of burning surface by Ni, C, and NiO mixture. This mixture sinters together and is blown into the flame zone by oxygen, leading to the hard-to-burn fragments ultimately. The difference of regression rate improvement in HTPB + $Ni(acac)_2$ between high and low oxygen mass flux results from the influence of combustion heat on convective heat transfer, which dominates the combustion behavior of fuel grains [10]. In high oxidizer mass flux zone, the reduction of combustion heat in loaded formulations induced by the

addition of $Ni(acac)_2$ severely deteriorates the convective heat transfer. This deterioration partially off sets the catalytic effect of $Ni(acac)_2$ on HTPB-based fuels, resulting in an insignificant increase in the regression rate. Nevertheless, the influence of convective heat transfer on combustion is greatly reduced in low oxidizer mass flux, leading to an alleviated deterioration on combustion caused by the reduction of combustion heat.

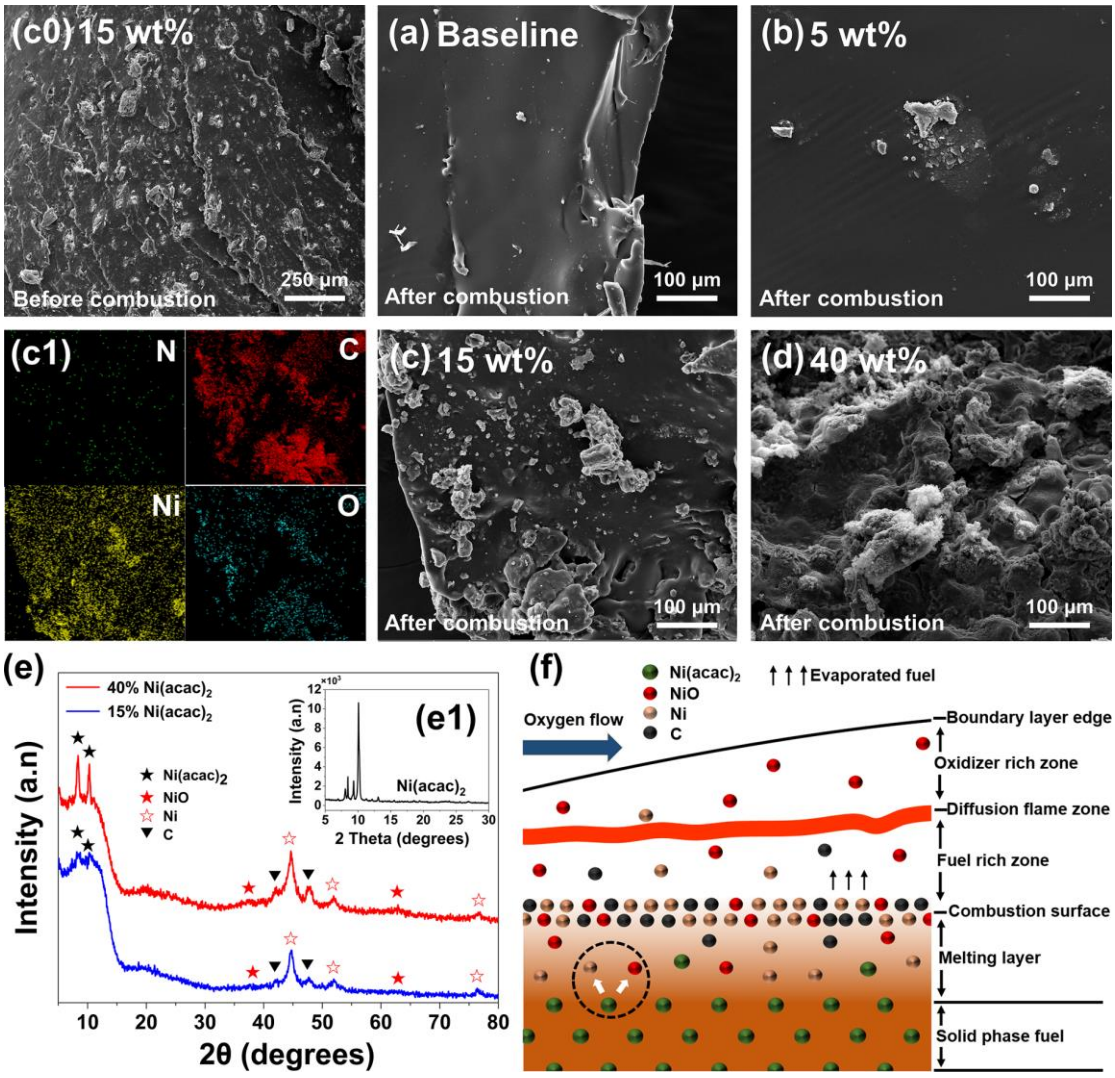

Fig. 11. SEM analyses of (a) baseline, (b) 5%, (c) 15%, (d) 40% $Ni(acac)_2$ after combustion termination and (c0) HTPB + 15% $Ni(acac)_2$ before combustion; (c1) EDS mapping results of HTPB + 15% $Ni(acac)_2$ after terminating combustion; (e) XRD

spectra of HTPB + $Ni(acac)_2$ with 15 wt% and 40 wt% (after combustion termination), and (e1) $Ni(acac)_2$ pristine material; (f) schematic of the combustion mechanism in HTPB + $Ni(acac)_2$ fuels.

4. Conclusion

This paper discusses the effects of the introduction of $Ni(acac)_2$ in HTPB-based fuels for hybrid rocket propulsion. Experimental results show that $Ni(acac)_2$ can catalyze the pyrolysis of HTPB-based formulations, hence significantly increase the regression rate even at a low content (5% $Ni(acac)_2$ enhances the regression rate by 25.5% at G_{OX} = 50 kg/m^{2}s). Experimental results testify that the catalytic action is exerted by Ni^{2+} in $Ni(acac)_2$, and NiO produced from the oxidative decomposition of $Ni(acac)_2$. On the other hand, with the introduction of relatively high $Ni(acac)_2$ mass fractions, a reduction of combustion heat is noted together with the insurgence of surface phenomena partially contrasting the fuel regression. Under the investigated conditions, regression rate enhancement shows a faint dependence from the additive mass fraction in the fuel. Under the investigated conditions, 5 wt% $Ni(acac)_2$ significantly affects HTPB decomposition process, providing enhanced regression rates. Yet, HTPB + 40 wt% $Ni(acac)_2$ shows a regression rate reduction with respect to the baseline. While a detailed analyses of the combustion products is needed in order to identify an optimal $Ni(acac)_2$ mass fraction for HTPB-based formulations, in the tested conditions the maximum regression rate increase and the lowest data scattering is achieved by HTPB + 15 wt% $Ni(acac)_2$.

Achieved experimental results suggest that $Ni(acac)_2$ can be a suitable candidate for

regression rate performance enhancement in HTPB-based formulations. Future developments of the presented work will include an evaluation of the effects of NiO and other transition metal oxides on the combustion mechanism of solid fuels for hybrid propulsion and an application of this strategy to other solid fuel matrixes or reinforced polymers.

Author Contributions

R. Shen conceived the research project. W. Zhang supervised the project. H. Yu and S. Chen designed the methods and experimental setups. H. Yu, and X. Yu implemented the whole experiments. H. Yu analyzed the results and wrote the original draft. C. Paravan and L. T. DeLuca provided some modification recommendations. All authors discussed and revised the paper.

Declaration of Competing Interest

The authors declare that they have no known competing financial interests or personal relationships that could have appeared to influence the work reported in this paper.

Acknowledgment

This work was supported by the National Natural Science Foundation of China (Grant No. 12074187) and the Fundamental Research Funds for the central Universities (Grant no. 30919012102, 30919011404, 30918011315).

Reference

[1] M.J. Chiaverini, Encyclopedia of aerospace engineering, John Wiley & Sons, Ltd.

USA, 2010. https://doi.org/10.1002/9780470686652.eae113.

[2] M.J. Chiaverini, K.K. Kuo, Fundamentals of hybrid rocket combustion and propulsion, American Institute of Aeronautics and Astronautics, USA, 2007. https://doi.org/10.2514/4.866876.

[3] Q. Zhang, Y. Shu, N. Liu, X. Lu, Y. Shu, X. Wang, et al. Hydroxyl terminated polybutadiene: chemical modification and application of these modifiers in propellants and explosives, Cent. Eur. J. Energ. Mater. 16 (2019) 153-193. http://www.wydawnictwa.ipo.waw.pl/cejem/Vol-16-Number-2-2019/CEJEM_00917.pdf.

[4] A. Aoki, A.B. Fukuchi, Development of low cost fuels for hybrid rocket engine, 46th AIAA/ASME/SAE/ASEE Joint Propulsion Conference & Exhibit (2010), 6638 https://doi.org/10.2514/6.2010-6638.

[5] Q. Zhou, S. Jie, B.C. Li, Preparation of Hydroxyl-Terminated Polybutadiene with High Cis-1,4 Content, Ind. Eng. Chem. Res. 53 (2014), 17884-17893. https://doi.org/10.1021/ie503652g.

[6] X. Sun, H. Tian, Y. Li, N. Yu, G. Cai, Regression rate behaviors of HTPB-based propellant combinations for hybrid rocket motor, Acta Astronaut. 119 (2016) 137-146. https://doi.org/10.1016/j.actaastro.2015.11.015.

[7] L.T. DeLuca, L. Galfetti, F. Maggi, G. Colombo, L. Merotto, M. Boiocchi, et al. Characterization of HTPB-based solid fuel formulations: Performance, mechanical properties, and pollution, Acta Astronaut. 92 (2013) 150-162. https://doi.org/10.1016/j.actaastro.2012.05.002.

[8] G.A. Risha, B.J. Evans, E. Boyer, R.B. Wehrman, K.K. Kuo, Nano-sized aluminum and boron-based solid fuel characterization in a hybrid rocket engine, 39th AIAA/ASME/SAE/ASEE joint propulsion conference and exhibit (2003), 4593. https://doi.org/10.2514/6.2003-4593.

[9] S. Chen, Y. Tang, H. Yu, L. Bao, W. Zhang, L.T. DeLuca, et al. The rapid H_2 release from AlH_3 dehydrogenation forming porous layer in AlH_3/hydroxyl-terminated polybutadiene (HTPB) fuels during combustion, J. Hazard. Mater. 371 (2019) 53-61. https://doi.org/10.1016/j.jhazmat.2019.02.045.

[10] C. Paravan, Nano-Sized and Mechanically Activated Composites: Perspectives for Enhanced Mass Burning Rate in Aluminized Solid Fuels for Hybrid Rocket Propulsion. Aerospace 6 (2019), 127. doi:10.3390/aerospace6120127.

[11] P. George, S. Krishnant, P.M. Varkey, M. Ravindran, L. Ramachandran, Fuel regression rate enhancement studies in HTPB/GOX hybrid rocket motors, 34th AIAA/ASME/SAE/ASEE Joint Propulsion Conference and Exhibit (1998), 3188. https://doi.org/10.2514/6.1998-3188.

[12] O. Einav, A. Peretz, B. Hashmonay, A. Birnholz, Z. Sobe, Development of a lab-scale system for hybrid rocket motor testing, 45th AIAA/ASME/SAE/ASEE Joint Propulsion Conference & Exhibit (2009), 4888. https://doi.org/10.2514/6.2009-4888.

[13] S. Chen, Y. Tang, H. Yu, X. Guan, L.T. DeLuca, W. Zhang, et al. Combustion enhancement of hydroxyl-terminated polybutadiene by doping multiwall carbon nanotubes, Carbon. 144 (2019) 472-480. https://doi.org/10.1016/j.carbon.2018.12.063.

[14] Y. Wang, L. Jiang, J. Dong, B. Li, J. Shen, L. Chen, et al. Three-dimensional

network structure nitramine gun propellant with nitrated bacterial cellulose, J. Mater. Res. Technol. 9 (2020) 15094-15101. https://doi.org/10.1016/j.jmrt.2020.10.097.

[15] Y. Tang, S. Chen, W. Zhang, R. Shen, L.T. DeLuca, Y. Ye, Mechanical Modifications of Paraffin‐based Fuels and the Effects on Combustion Performance. Propellants, Explos., Pyrotech. 42 (2017) 1-11. https://doi.org/10.1002/prep.201700136.

[16] J.C. Thomas, J.M. Stahl, A.J. Tykol, F.A. Rodriguez, E.L. Petersen, Hybrid rocket studies using HTPB/paraffin fuel blends in gaseous oxygen flow, 7th European Conference for Aeronautics and Space Sciences (EUCASS) (2015), 1-13. https://doi.org/10.1016/j.combustflame.2021.02.032.

[17] J.C. Thomas, Mixed HTPB/paraffin fuels and metallic additives for hybrid rocket applications, Doctoral dissertation (2018). https://hdl.handle.net/1969.1/192059.

[18] J.C. Thomas, C. Paravan, J.M. Stahl, A.J. Tykol, F.A. Rodriguez, L. Galfetti, et al. Experimental evaluation of HTPB/paraffin fuel blends for hybrid rocket applications, Combust. Flame 229 (2021) 111386. https://doi.org/10.1016/j.combustflame.2021.02.032.

[19] Y. Liu, S. Jin, H. Yang, S. Li, W. Xie, Y. Zhao, et al. Application of 3D energetic metal-organic frameworks containing Cu as the combustion catalyst to composite solid propellant, Combust. Flame 225 (2021) 57-64. https://doi.org/10.1016/j.combustflame.2020.10.035.

[20] Y. Wang, J. Dai, J. Xu, Y. Shen, C. Wang, Y. Ye, et al. Experimental and numerical investigations of the effect of charge density and scale on the heat transfer behavior of

Al/CuO nano-thermite, Vacuum 184 (2021) 109878. https://doi.org/10.1016/j.vacuum.2020.109878.

[21] D. Zhang, C. Cao, S. Lu, Y. Cheng, H. Zhang, Experimental insight into catalytic mechanism of transition metal oxide nanoparticles on combustion of 5-Amino-1H-Tetrazole energetic propellant by multi kinetics methods and TG-FTIR-MS analysis, Fuel 245 (2019) 78-88. https://doi.org/10.1016/j.fuel.2019.02.007.

[22] D. Zhang, S. Lu, C. Cao, C. Liu, L. Gong, H. Zhang, Impacts on combustion behavior of adding nanosized metal oxide to CH_3N_5-$Sr(NO_3)_2$ propellant, Fuel 191 (2017) 371-382. https://doi.org/10.1016/j.fuel.2016.11.074.

[23] Y. Xu, Y. Wang, Y. Zhong, G. Lei, Z. Li, J. Zhang, et al. Transition metal complexes based on hypergolic anions for catalysis of ammonium perchlorate thermal decomposition, Energy Fuels 34 (2020) 14667-14675. https://doi.org/10.1021/acs.energyfuels.0c02570.

[24] K. Kishore, M.R. Sunitha, Effect of transition metal oxides on decomposition and deflagration of composite solid propellant systems: A survey, AIAA J. 17 (1979) 1118-1125. https://doi.org/10.2514/3.61286.

[25] G. Moroi, C. Ciobanu, Aspects of polyesterurethane interaction with metallic ions: II. Synthesis and thermal behavior of polyurethane interaction products with manganese and copper ions, Thermochim. Acta 385 (2002) 153-162. https://doi.org/10.1016/S0040-6031(01)00713-4.

[26] O. Terakado, H. Yanase, M. Hirasawa, Pyrolysis treatment of waste polyurethane foam in the presence of metallic compounds, J. Anal. Appl. Pyrolysis 108 (2014) 130-

135. https://doi.org/10.1016/j.jaap.2014.05.008.

[27] J. Pavlicˇevic´, M. Špírková, O. Bera, M. Jovicˇic´, B. Pilic´, S. Baloš, et al. The influence of ZnO nanoparticles on thermal and mechanical behavior of polycarbonate-based polyurethane composites, Composites, Part B 60 (2014) 673-679. https://doi.org/10.1016/j.compositesb.2014.01.016.

[28] A. Laachachi, M. Ferriol, M. Cochez, D. Ruch, J.-M. Lopez-Cuesta, The catalytic role of oxide in the thermooxidative degradation of poly(methyl methacrylate)-TiO_2 nanocomposites, Polym. Degrad. Stab. 93 (2008) 1131-1137. https://doi.org/10.1016/j.polymdegradstab.2008.03.006.

[29] K.P. Cardoso, L.F.A. Ferrão, E.Y. Kawachi, J.S. Gomes, M.Y. Nagamachi, Ballistic performance of paraffin-based solid fuels enhanced by catalytic polymer degradation, J. Propul. Power 35 (2019) 115-124. https://doi.org/10.2514/1.B36977.

[30] V. Vand, A theory of the irreversible electrical resistance changes of metallic films evaporated in vacuum, Proc. Phys. Soc. 55 (1943) 222. DOI: 10.1088/0959-5309/55/3/308.

[31] A.K. Burnham, R.L. Braun, Global kinetic analysis of complex materials, Energy Fuels 13 (1999) 1-22. https://doi.org/10.1021/ef9800765.

[32] K. Miura, T. Maki, A simple method for estimating f (E) and k_0 (E) in the distributed activation energy model, Energy Fuels 12 (1998) 864-869. https://doi.org/10.1021/ef970212q.

[33] H.E Kissinger, Variation of peak temperature with heating rate in differential thermal analysis, J. Res. Natl. Bur. Stand. 57 (1956) 217-221.

https://nvlpubs.nist.gov/nistpubs/jres/057/4/V57.N04.A05.pdf.

[34] R. Molina, M. A. Centeno, G. Poncelet, α-Alumina-supported nickel catalysts prepared with nickel acetylacetonate. 2. A study of the thermolysis of the metal precursor, J. Phys. Chem. B 103 (1999) 11290-11296. https://doi.org/10.1021/jp9907286.

[35] J.S. Schubert, J. Popovic, G.M. Haselmann, S.P. Nandan, J. Wang, A. Giesriegl, et al. Immobilization of Co, Mn, Ni and Fe oxide co-catalysts on TiO_2 for photocatalytic water splitting reactions, J. Mater. Chem. A 7 (2019) 18568-18579. https://doi.org/10.1039/C9TA05637H.

[36] I.V. Babich, Yu.V. Plyuto, A.D. Van Langeveld, J.A. Moulijn, Role of the support nature in chemisorption of $Ni(acac)_2$ on the surface of silica and alumina, Appl. Surf. Sci. 115 (1997) 267-272. https://doi.org/10.1016/S0169-4332(96)01016-1.

[37] Y. Goto, K. Taniguchi, T. Omata, S. Otsuka-Yao-Matsuo, N. Ohashi, S. Ueda, et al. Formation of Ni_3C nanocrystals by thermolysis of nickel acetylacetonate in oleylamine: characterization using hard X-ray photoelectron spectroscopy, Chem. Mater. 20 (2008) 4156-4160. https://doi.org/10.1021/cm703644x.

[38] H. Abdel-Khalek, M.I. El-Samahi, A.M. El-Mahalawy, Influence of post-deposition annealing on structural, morphological and optical properties of copper (II) acetylacetonate thin films, Spectrochim. Acta, Part A. 202 (2018) 389-400. DOI: 10.1016/j.saa.2018.05.071.

[39] Z. Zhang, X. Fu, H. Yu, W. Tao, C. Mao, P. Chen, et al. Enhanced the thermal conductivity of hydroxyl-terminated polybutadiene (HTPB) composites by graphene-

silver hybrid, Compos. Commun. 24 (2021) 100661. https://doi.org/10.1016/j.coco.2021.100661.

[40] Y. Tang, S. Chen, W. Zhang, R. Shen, L. T. Deluca, Y. Ye, Mechanical modifications of paraffin-based fuels and the effects on combustion performance, Propellants, Explos., Pyrotech. 42 (2017): 1268-1277. https://doi.org/10.1002/prep.201700136

[4] J. D. DeSain, B. B. Brady, K. M. Metzler, T. J. Curtiss, T. V. Albright, Tensile tests of Paraffin Wax for Hybrid Rocket Fuel Grains. 45th AIAA/ASME/SAE/ASEE Joint Propulsion Conference & Exhibit, Denver, CO, USA, August 2–5, 2009, p. 5115. https://doi.org/10.2514/6.2009-5115

https://doi.org/10.2514/6.2010-7031 **46th AIAA/ASME/SAE/ASEE Joint Propulsion Conference & Exhibit ……25 - 28 July 2010, Nashville, TN Effect of Paraffin-LDPE Blended Fuel in**

Hybrid Rocket Motor

Soojong Kim1, Jungpyo Lee2, Heejang Moon3, Honggye Sung4, JinkonKim **AIAA 2010-7031**

[1] M. Zhang, F. Zhao, Y. Wang, X. Chen, Q. Pei, H. Xu, etc. Evaluation of graphene-ferrocene nanocomposite as multifunctional combustion catalyst in AP-HTPB propellant, Fuel 302 (2021), 121229. https://doi.org/10.1016/j.fuel.2021.121229.

[2] J. Jeong, V.K. Bhosale, S. Kwon, Ultrafast igniting, low toxicity hypergolic hybrid solid fuels and hydrogen peroxide oxidizer, Fuel 286 (2021) 119307. https://doi.org/10.1016/j.fuel.2020.119307.

[3] V.K. Bhosale, J. Jeong, S. Kwon, Ignition of boron-based green hypergolic fuels with hydrogen peroxide, Fuel 255 (2019) 115729. https://doi.org/10.1016/j.fuel.2019.115729.

[4] C. Dennis, B. Bojko, On the combustion of heterogeneous AP/HTPB composite

propellants: A review, Fuel 254 (2019) 115646. https://doi.org/10.1016/j.fuel.2019.115646.
[5] K. K, S. Prema, K. Iyanar, L.P. Pandureng, Mechanistic studies on the effect of ferrocene bonding agents in composite solid propellants, Fuel 73 (1994) 1583-1593. https://doi.org/10.1016/0016-2361(94)90136-8.
[6] L. Song, F. Zhao, S. Xu, X. Ju, C. Ye, ReaxFF study on combustion mechanism of ethanol/nitromethane, Fuel, 303 (2021) 121221, https://doi.org/10.1016/j.fuel.2021.121221.
[7] J. John, P. Nandagopalan, S.W. Baek, A. Miglani, Rheology of solid-like ethanol fuel for hybrid rockets: Effect of type and concentration of gellants, Fuel 209 (2017) 96-108. https://doi.org/10.1016/j.fuel.2017.06.124.